AUTOMATED IMAGE ANALYSIS FOR ELECTRON MICROSCOPY SPECIMEN ASSESSMENT

Nicolas Coudray, Jean-Luc Buessler, Hubert Kihl, Jean-Philippe Urban

Laboratoire MIPS, Université de Haute Alsace
4, rue des Frères Lumière, 68093 Mulhouse, France
phone: +(33)389-33-64-32, email: nicolas.coudray@uha.fr

ABSTRACT

This paper presents an automatic image analysis process that emulates the decision of a microscopist in evaluating 2D crystallized proteins. The purpose of the process is to locate the interesting regions in each image and finally assess if the crystallization succeeded. A top-down approach decomposes the process into three steps, corresponding to levels of magnification of the transmission electron microscope. For the first step (low magnification), the automatic process efficiently evaluates the quality of the grid where the specimen relies. In the second step (medium magnification), the protein-embedded membranes are analyzed. The images are classified with a histogram-based analysis to reject uninteresting images and the remaining ones are processed with an edge-based algorithm to localize the membranes and select the potentially crystallized areas. In the last step (high magnification), an algorithm extracts automatically the peaks from the diffraction pattern of the previously selected areas. The tests show encouraging results.

1. INTRODUCTION

Membrane proteins are part of all living organisms and understanding their functions is a big challenge. To facilitate the study of their structure, 2D-crystallization arranges proteins into lipid bi-layers (artificial membranes) upon detergent removal [6]. However, determining the conditions for crystallization is a strenuous process that requires a large amount of sample preparation that has to be analysed with a Transmission Electron Microscope (TEM). It is therefore important to develop on-line tools that can routinely assess the results and the quality of the crystals.

Some efforts have been placed on the automatic screening of specimen with a microscope [3, 4]. Though some tools are being developed for 3D-crystallization [8] and single particles analysis [11], the required automatic analysis of the images is still at its infancy, especially for 2D-crystallization. The GRACE package has been developed by Oostergetel et al. [4] for 2D-crystallization of proteins: the screening is automatic or semi-automatic but the decisions and analysis are to be done manually. Later, the Leginon system, mainly developed for single particle screening in cryo-microscopy, was adapted for automatic detection of 2D-crystals. The process was however too much focused on well contrasted and mostly rectangularly crystallized catalase proteins [5] to be valid for the examination of other kinds of crystal experiments. The automatic and on-line analysis of images is thus an emerging field of application for image processing.

The success of the crystallization is shown by the peaks in the diffraction pattern at high magnification (around 5 Å/pixel). At this magnification, the screening of a 3 mm diameter sample grid is just unrealistic (time and energy consuming and inefficient when the specimen is rare). Therefore, the grid has to be screened at lower magnifications to direct the microscope to the regions of interest where proteins are likely to be crystallized.

In this paper we introduce and describe a top-down approach that decomposes the process into three steps, corresponding to the levels of magnification at which the images are acquired. We contribute at each step by proposing an automated image analysis that will result in the selection of areas of interest to be explored at the next level of magnification.

The top-down approach applied is similar to the common three-step method used when the samples are studied manually or with semi-automatic tools [4]. Tools need to be developed to analyse three types of images:

(1) Low magnified images are processed to assess the overall quality of the grid and detect the squares where the carbon film is intact to inform where the higher magnified images should be acquired. This process is developed in section 2.

(2) Images acquired at medium magnification (about x5,000) are used to localize the membranes and select the potentially crystallized areas. This part, presented in section 3, is subdivided into two steps: a pre-classification of the image based on the histogram to reject the irrelevant images, and an edge-based segmentation of the selected images for a fast membrane localization and area selection.

(3) In section 4, high magnified images (about x50,000) of potentially crystallized areas are analyzed to detect possible diffraction peaks.

2. TEM GRID ASSESSMENT AT LOW MAGNIFICATION

Samples are placed on a thin carbon film and a 3 mm diameter copper grid used in TEM. Grids with completely undamaged carbon film are quite rare and that is why an automatic analysis of their quality is essential to avoid losing time analysing areas where the film is damaged.

Zhang *et al.* [9] developed a process for grid assessment in cryo-microscopy that relies on a user-define reference. The challenge here was to develop an algorithm adapted for grid assessment in electron crystallography that is completely independent from any user input.

To achieve this goal, we have developed an original method mainly based on histogram analysis. It consists of a grid identification step and a first on-line assessment step, and a second optional assessment step based on information gathered during the first two steps.

As a preliminary step, a global histogram analysis (Figure 1) is done to identify the grid squares: the relative opacity of the copper to electrons creates a sharp peak at the beginning of the histogram. The threshold is set at the first local minima after this peak.

Then, the analysis of the carbon film at each square relies on the following observations. Four classes of squares can be identified (Figure 2):
(A) the undamaged squares where membranes are big and contrasted enough to be visible
(B) the undamaged squares where the membranes are too small to be visible
(C) the squares where the film is broken
(D) the squares where the film is completely missing.

The squares of type (A) and (C) can easily be discriminated by a process that is applicable 'on-line'. The process is based on local histogram segmentation (Figure 2): for each square, the last peak P_{last} of the histogram is identified and thresholded. This peak represents the background, the brightest pixels. For squares of type (A), the surface covered by those pixels has 'holes' due to the darker, large and visible membranes. The area enclosed in the convex envelop of the background is approximatively equal to the size of the square (in the implementation, an error of +/-5% is allowed). For squares of type (C), the area (and convex area) covered by the brightest pixels do not cover the whole square. The squares of class (C) are the more important to reject since broken films can look like membranes at medium magnification analysis, which would lead to false positives. For squares of types (B) and (D), the segmented pixels cover the whole square. The only visible difference between square (B) and (D) are their mean gray level that is slightly darker when the carbon is present. As a consequence, since it is not possible to *a priori* know the typical gray level when the film is absent or present, these two classes cannot be distinguished in the first quality assessment, unless a reference has been pre-entered by the user.

To avoid any external input, we have developed a second quality assessment based on the information gathered during the first quality assessment: after several grid squares have been acquired, we have statistical information about the mean gray level of P_{last} for squares of type (A) and (C), thus the mean gray level of the background pixels when the carbon film is present and absent. This information is used in the second quality assessment step to identify, by the gray level analysis, the squares of type (B) and (D). If there is no square of class (A), the limit gray level for square rejection is chosen by:

$$T_{empty} = \overline{GL}_C - 2 \times STD_C \,, \qquad (2)$$

with $\overline{GL}_C$ and STD_C being the mean and standard deviation of the gray level distribution of the background pixels identified in class (C). The first step also gives statistical information about the shape and the size of the squares which can be used for checking in the second quality assessment.

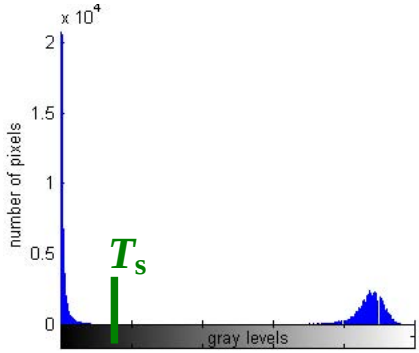

Figure 1 Typical global histogram of a low magnified image and the threshold T_s for the square segmentation

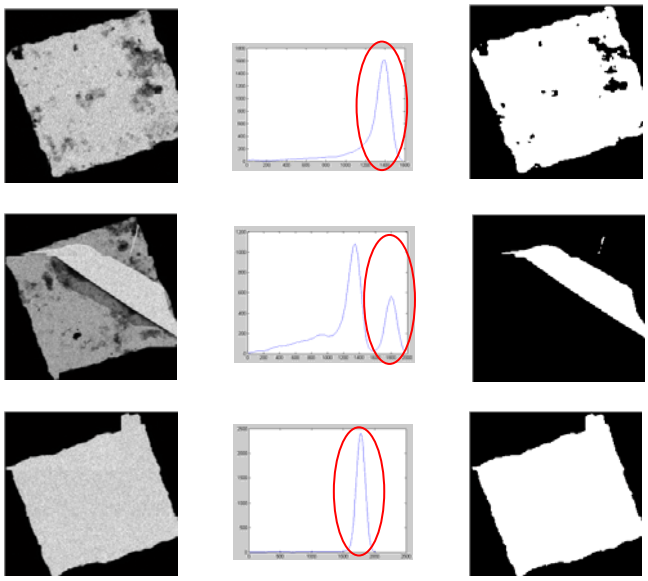

Figure 2 The different classes of squares: line 1: class (A) for undamaged film and visible membranes; line 2: class (C) for damaged film; line 3: class (B) or (D): carbon and small membranes or no carbon at all; column 1: gray level images; column 2: aspect of the local histogram and segmentation of the last peak; column 3: brightest pixels segmented. The grid square size is ≈ 60 x 60 µm.

3. MEDIUM MAGNIFICATION ANALYSIS

Histogram-based pre-Classification of Images

The image pre-classification proposed is a fast way to reject images that are not worth being treated. This step is based on the histogram analysis of the smoothed images.

The following classes of histograms are proposed: expected histogram, aggregate-like histogram, grid-like histogram and noise-like histogram:

(1) The images with an expected histogram (Figure 3) are the only that are worth being analyzed. The histogram is characterized by a main bright peak located at the right-side of the histogram. Indeed, though negative staining locally enhances the contrast, the histogram of the biological specimens cannot be clearly separated from the background by a simple threshold.

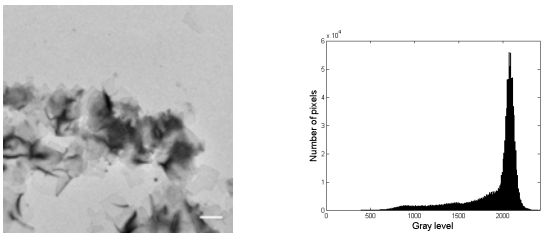

Figure 3 Expected image (scale bar: 1 µm) and histogram

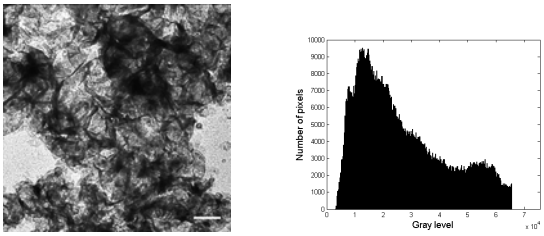

Figure 4 Aggregate-like image (scale bar: 1 µm) and histogram

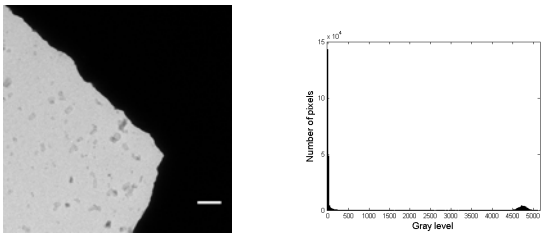

Figure 5 Grid-like image (scale bar: 1 µm) and histogram

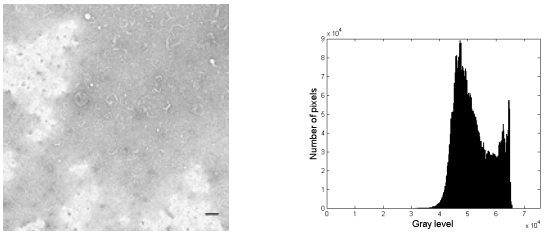

Figure 6 Noise-like image (scale bar: 1 µm) and histogram

(2) Aggregate-like histograms (Figure 4) occur when membranes are so amassed that the image is not worth being analyzed. The bigger the aggregates, the higher the quantity of diffracted and scattered electrons, the darker the gray level of the image. The main two peaks of the histogram are studied: if the height of the darkest peak (representing aggregates) is too high, then, the image is rejected. The limit height has been fixed to half the height of the main bright peak.

(3) Grid-like histograms (Figure 5) belong to images where the mesh grid is visible. Thus, the area occupied by the carbon film where the membranes could be seen is small or absent. The grid is opaque to electrons and a peak is visible at the very left-side of the histogram. Images are classified in this class if their histogram begins with a maximum. The grid is then segmented by a threshold placed on the first local minimum after the first peak. If more than half of the image is covered with grid, the image is rejected and not analyzed.

(4) Noise-like histograms (Figure 6) inform on different noises: detergent used for the membrane reconstruction remaining, important artifacts or holes in the carbon due to over-exposition to the electron beam. The noise-free histogram is identified if there are several peaks on the right-side of the histogram and is the main peak is not symmetric.

Region of Interest Selection

The images with an expected histogram are then analyzed to identify the membranes and the regions to be analyzed at high magnification. The outputs of this step are the coordinates of the selected ROIs (Regions Of Interest).

Segmentation of biological specimens is difficult, especially in these cases where the contrast, the gray level, the size and the shape of the objects vary greatly. Though negative staining with heavy metal is used, the locally enhanced contrast is still not sufficient to clearly separate the membranes from the background with a simple threshold method. Since the membranes are visible thanks to their local contrast, the approach relies on edge-detection of the images. The ROIs are selected near the edges found. The size *MxM* of the ROIs is chosen to be at least as large as the high magnified images to avoid redundant selections. Thus, if the size of the image is *NxN* pixels at medium magnification of 5,000, then, to represent the areas at the high magnification of 50,000, the size *MxM* of the ROI is defined by equation (1):

$$M = \frac{N}{10} \tag{1}$$

Thus, the steps of the process are as follows:

(a) Edge detection of the smoothed image is processed with the Prewitt filter.

(b) The bounding box of each object (connected pixels) is calculated.

(c) Each bounding box is sub-segmented into *MxM* squares (Figure 7, left). Sub-segmentation of the bounding boxes instead of sub-segmentation of the whole image allows a better positioning of the ROIs around the edges.

(d) The number of squares is then reduced by removing less interesting regions:

- A threshold is set to assure that the quantity of edges in the ROI pixels detected is high enough to be interesting.
- Overlapped selections are limited by rejecting the stronly redundant squares
- In the gray level image, if the gray level of the area is too dark, the *MxM* square is rejected. It is probably an aggregate or an artifact because the interesting membranes are low contrasted. A square is rejected if its mean gray level is not included near the bright Gaussian-like peak of the histogram.

The remaining *MxM* squares (Figure 7, right) are the ROIs retained for high magnification analysis.

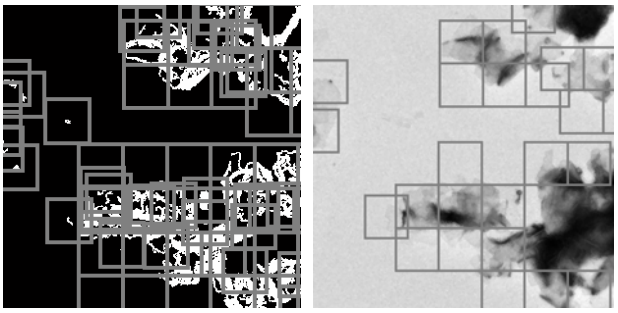

Figure 7 (*left*) *MxM* squares selection after edge detection (step 3.1) and (*right*) ROIs selected after squares analysis (step 3.2). Image size is ≈ 10 x 10 µm.

4. HIGH MAGNIFICATION ASSESSMENT OF THE DIFFRACTION PATTERNS

The images acquired at a high magnification of 50,000 (about 5 Å/pixel) are potentially crystallized membranes. The Fourier transform of the image is used to detect the diffraction peaks that will attest the presence of crystals [4, 10].
The peak identification is made difficult by the ring-shaped noise visible in the reciprocal space. These rings, called the Thon rings [7], are due to the Contrast Transfer Function (CTF) of the microscope. A simple threshold of the peaks is therefore not suitable. The process proposed to automatically detect the peaks is a 2-step method that does not require any *a priori* knowledge on the lattice, on the CTF or on the microscope setup: the background of the power spectrum image is firstly evaluated to remove the effect of the Thon rings and then, the image is thresholded to identify the peaks.

The mean radial profile can be used for background estimation (MRC program) or for CTF estimation by rotational averaging of the power spectrum [2]. The value of the mean radial profile V_f can be expressed as:

$$Vf = \frac{\sum_{\theta}(x_{f,\theta}, y_{f,\theta})}{n_{\theta}} \qquad (2)$$

where f is the frequency, n_θ the number of pixels of coordinates $(x_{f,\theta}, y_{f,\theta})$ at the same frequency f but different angles θ. V_f is used as an estimate of the background which is subtracted from the Fourier Transform image. The resulting image is then segmented by thresholding (Figure 8 and Figure 9). The mean profile is bound to represent the background, but its value can be slightly biased at frequencies where bright peaks of diffractions are located. Thus, to reduce this effect, the extremum values are removed: for each f, the vector $[x_{f,\theta}, y_{f,\theta}]$ is sorted and V_f is calculated with the median values.

The implementation of the process has been speeded up by reducing the analyzed window. Since the staining limits the resolution to 20 Å, the analysis was restricted to the lower frequencies, represented by the circle C_{20} on Fig. 8, where the radius R_{rc} is given by:

$$R_{rc} = R_{fft} \times \frac{4\text{Å}}{20\text{Å}} \qquad (3)$$

with R_{fft} being half the size of the Fourier window, 4 Å the pixel size in the real plan and 20 Å the resolution at C_{20}. Moreover, thanks to the symmetry, the mean profile can be calculated on half circle from $\theta = [0 ; \pi]$.

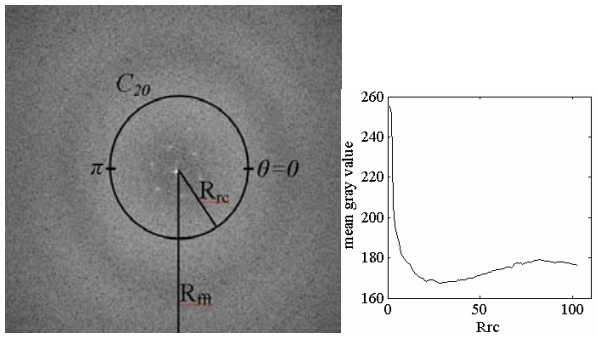

Figure 8 Diffraction pattern (*left*) with R_{fft} is half the window size, C_{20} is the circle of radius R_{rc} and limit for a 20 Å resolution; Mean radial profile (*right*).

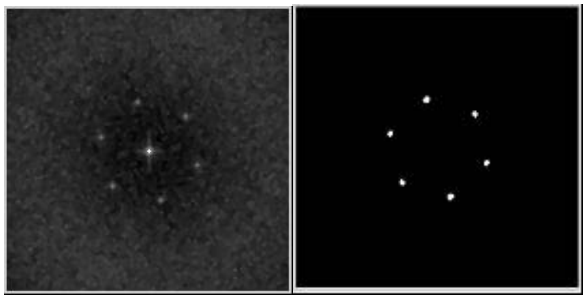

Figure 9 Windows enclosing C_{20} after background removal (*left*) and then thresholding (*right*)

5. RESULTS AND DISCUSSION

The algorithm at low magnification has been tested on images from two different kinds of grids. The automatic classification is very close to the manual classification (Table 1 and Table 2). There are very few false negatives mainly due to the threshold chosen to reject the smallest squares (the size should be at least 75 % of the size of the biggest square), and no false positive which is very good since these false detection would be more problematic.

Table 1. Comparison between manual and automatic classification of images from two grids

A/ Grid 1

		Manual Classification	
		Squares selected	Squares rejected
Automatic classification	Squares selected	166	
	Squares rejected	2	19

B/ Grid 2

		Manual Classification	
		Squares selected	Squares rejected
Automatic classification	Squares selected	164	
	Squares rejected	5	125

In the medium magnification step, the pre-classification of the images according to the histogram is a valuable step that avoids losing time processing images where little or no information can be extracted from further image processing. Different images acquired with different microscopes (Hitachi H-7000, Hitachi H-8000, Philips CM200 and FEI Tecnai F30) have been tested and the results show no discrepancy in the classification; only some images where the membranes are more or less aggregated can lead to discussion whether further analysis would be useful or not.

Though an objective assessment of the ROI selection is difficult, it can be considered that it meets its primary goal of reducing the high magnification screening time by disposing of aggregates and empty regions. Furthermore, it can be noticed that the selected ROIs do not vary significantly under image translation, rotation or scaling. We are currently developing a multi-scale approach based on gradient amplitude analysis for better segmentation [1]. It aims to extracts more information on the membranes like the shape, the size, and the degree of aggregation. It would also allow a better positioning of the ROIs in the middle of the larger membranes rather than on the edge.

As for the high magnification algorithm, test results compared with visual inspection give similar results to detect whether there are diffraction peaks or not. Diffraction spots can still be detected when only a quarter of the 1000x1000 pixel image of crystallized membranes is processed. A quality assessment can then be based on several parameters [10]. In the developed analysis, the number of peaks and the resolution of the peaks have been chosen to inform the user on the diffraction. The microscope was setup to reduce the astigmatism of the images. If it is too high, then, it should be corrected before the detection of the peaks that relies on the radial profile.

6. CONCLUSION

We presented an automatic image analysis process to assess the crystallization of 2D-membranes. At the low magnification, the algorithm develop is completely independent from any reference image and gives very good results. The first analysis at medium magnification classifies the images according to their histogram to efficiently reject those that are not worth being analyzed. Then, an original edge-based algorithm selects the potentially crystallized areas. This part is still being investigated to enhance the segmentation and the amount of information that could be extracted at this magnification. Finally, the high magnification process detects peaks in the diffraction pattern to identify the crystals.

Acknowledgments. This work was supported by the EU 6th framework (HT3DEM, LSHG-CT-2005-018811, in collaboration with the Biozentrum of Basel and the Max-Planck Institute for Biochemistry in Martinsried who provided the TEM images.

REFERENCES

[1] N. Coudray, J.-L. Buessler, H. Kihl, and J.-P. Urban, "TEM images of membranes: a multiresolution edge-detection approach for watershed segmentation," in *Physics in Signal and Image Processing (PSIP)*, Mulhouse, France, 2007.

[2] S. P. Mallick, B. O. Carragher, C. S. Potter, and D. J. Kriegman, "ACE: Automated CTF Estimation," *Ultramicroscopy*, vol. 104, pp. 8-29, August 2005.

[3] S. Nickell, F. Förster, A. Linaroudis, W. Del Net, F. Beck, R. Hegerl, W. Baumeister, and J. M. Plitzko, "TOM software toolbox: acquisition and analysis for electron tomography," *Journal of Structural Biology*, vol. 149, pp. 227-234, March 2005.

[4] G. T. Oostergetel, W. Keegstra, and A. Brisson, "Automation of specimen selection and data acquisition for protein electron crystallography," *Ultramicroscopy*, vol. 74, pp. 47-59, July 1998.

[5] C. S. Potter, H. Chu, B. Frey, C. Green, N. Kisseberth, *et al.*, "Leginon: A System for Fully Automated Acquisition of 1000 Micrographs a Day," *Ultramicroscopy*, vol. 77, pp. 153-161, July 1999.

[6] H. Stahlberg, D. Fotiadis, S. Scheuring, H. Rémigy, T. Braun, K. Mitsuoka, Y. Fujiyoshi, and A. Engel, "Two-dimensional crystals: a powerful approach to assess structure, function and dynamics of membrane proteins," *FEBS Letters*, vol. 504, pp. 166-172, August 2001.

[7] F. Thon, "Phase contrast electron microscopy," *Electron Microscopy in Material Sciences*, pp. 571-625, 1971.

[8] J. Wilson, "Automated evaluation of crystallisation experiments," *Crystallography Reviews*, vol. 10, pp. 73-84, 2004.

[9] P. Zhang, A. Beatty, J. L. S. Milne, and S. Subramaniam, "Automated Data Collection with a Tecnai 12 Electron Microscope: Applications for Molecular Imaging by Cryomicroscopy," *Journal of Structural Biology*, vol. 135, pp. 251-261, September 2001.

[10] Z. Zhang, H. van den Bedem, N. K. Sauter, G. Snell, and A. M. Deacon, "Automated diffraction image analysis and spot searching for high-throughput crystal screening," *Journal of Applied Crystallography*, vol. 39, pp. 112-119, 2006 2006.

[11] Y. Zhu, B. Carragher, R. M. Glaeser, D. Fellmann, C. Bajaj, M. Bern, F. Mouche, F. d. Haas, R. J. Hall, D. J. Kriegman, S. J. Ludtke, S. P. Mallick, P. A. Penczek, A. M. Roseman, F. J. Sigworth, N. Volkmann, and C. S. Potter, "Automatic particle selection: results of a comparative study," *Journal of Structural Biology*, vol. 145, pp. 3-14, January 2004.